URSI AP-RASC 2019, New Delhi, India; 09 - 15 March 2019

RFI detection and mitigation in SAR data

Parikshit Parasher*(1), Krishna M Aggarwal(1), and V. M. Ramanujam(1)
(1) Space Applications Center, ISRO, Gujarat, 380058, India

Abstract

Radio Frequency Interference (RFI) are incoherent electromagnetic interference signals that appear as various kind of bright linear features in azimuth time range frequency diagram. RFI causes significant reduction in image contrast and introduces artifacts in image that may affect the polarimetric signatures and degrades the overall radiometric quality. Although the matched filtering which is an integral part of SAR data processing system has an inherent ability of interference suppression, yet high power RFI is still visible in Azimuth time Range frequency domain as bright stripes. It also introduces hazyiness in the image. The technique presented in this paper is a modified variant of an existing approach retaining the basic philosophy for RFI detection. It uses hypothesis testing based on z-test combined with Tukey biweights to estimate robust statistics for the purpose of RFI detection. Denoising of RFI mask is performed using statistical information of data. RFI correction is further performed using interpolation in magnitude based on local statistics.

1 Introduction

Radio frequency interference is an issue that affects the SAR signals, generally operating in Low frequency region e.g L,S and C band. Though RFI can affect signals in L,S and C band but L-band remains the most affected region. As per Recommendation ITU-R RS.577-7 of the ITU, active the allocation for Earth exploration satellite service (EESS) is from 1.215 GHz-1.3 GHz. The spectrum is allocated to Radio-navigation satellite service (RNSS) like GPS,GLONASS,GALILEO etc., radio-location service like air-surveillance radars and military air-defence radars and Amateur communication services [1]. Hence, in L-band there are various sources whose frequency overlaps with the frequency band of any microwave system making it more prone to RFI phenomenon. Examples of RFI cases in ESA C-band SAR (ERS-2 SAR) and EnviSat (5250-5350 MHz, burst RFI) has been presented earlier [1]. It seemed that these cases were possibly due to a military radar. Large parts of the ALOS Phased Array type L band SAR (PALSAR) acquisition over North America were affected with RFI due to the presence of long-range and short-range over-the-horizon radars of the North Warning System and radar stations operated by the FAA[2]. Section 2 describes methodology for RFI detection and correction. Section 3 depicts the algorithm flowchart. Section 4 discusses the RFI simulation exercise performed on RISAT-1 data alongwith the results. Section 5 summarizes the activity with scope for future work.

2 Methodology

RFI detection concept is based on the analysis of time-frequency characteristics of RFI's. The algorithm operates on $H(t,f)$ obtained by taking 1D Fourier transform of raw data in range direction. Time stationary narrow band(TSNB) and Time varying wide band(TVWB) RFI's are the end members of the family of large types of RFI's that can exist in SAR data [2].

2.1 TSNB RFI Detection

TSNB represents the RFI whose bandwidth is narrow and center frequency remains stationary with respect to azimuth time. In order to detect TSNB RFI, blocks of 256 azimuth lines are averaged. Using the averaged range power spectrum $|H(f)|^2$, population mean (μ) and population standard deviation (σ) are estimated made using the robust statistics i.e. Tukey biweights [3]. The sampling distribution of the statistic (i.e, mean) is assumed to be normally distributed. Next, the z-values corresponding to test statistic are obtained using [4],

$$Z = \frac{|H(f)|^2 - \mu}{SE} \tag{1}$$

Where, SE is known as standard error and it can be defined as standard deviation of the sampling distribution of a statistic. Mathematically [4],

$$SE = \frac{\sigma}{\sqrt{n}} \tag{2}$$

Where, n is the sample size, 256 in our case. The acceptance region corresponding to the null hypothesis that a given sample is an RFI is assigned a confidence level of $(1-\alpha) = 99.5\%$. Where, α, denotes the significance level and is defined as the probability of falsely rejecting null hypothesis. To detect RFI, identification of peaks is important, hence a one tailed Z-test is appropriate. The advantage of this method lies in the fact that the detection thresholds are not fixed rather dynamic depending on statistical properties of data.

2.2 TVWB RFI detection

TVWB represents the RFI whose bandwidth is wide and centre frequency varies with respect to azimuth time. A similar strategy is adopted as in case of TSNB with the variation that in this case the averaging is carried out in range frequency direction rather than azimuth time. If averaging is done in azimuth time than due to varying centre frequency the RFI will disappear in averaged spectra. Blocks of 100 range-frequency samples are averaged. The z-values can be defined as,

$$Z = \frac{|H(t)|^2 - \mu}{SE} \tag{3}$$

Where, $|H(t)|^2$ denotes averaged power spectrum along azimuth time. Sample size 'n' used in the calculation of SE is 100 here. Rest of the procedure remains similar to TSNB.

2.3 RFI correction

As a first step towards RFI correction, a single mask is generated based on TSNB and TVWB RFI detection. A thresholding is applied to the mask using statistical information of RFI unaffected data in order to denoise the mask. Further Denoising of the mask is performed based on a minimum RFI bandwidth and minimum RFI samples in range and azimuth directions respectively. As the RFI is incoherent[2], masked frequencies are now interpolated in magnitude based on local statistics retaining the original phase values.

3 Algorithm flowchart

Range-Doppler algorithm(RDA) has been used to focus SAR data during this work. This algorithm efficiently processes the SAR data in frequency domain. The time domain correlation operations, for range compression and azimuth compression, are replaced by the frequency domain multiplication operations. It allows the increased computational efficiency by applying RCM correction in Range-Doppler domain. RFI detection and correction is performed on raw data in Azimuth time range requency domian. After this operation, range compression is performed, followed by RCM correction and azimuth compression. The basic steps for the RFI detection and correction module are given in Figure 1.

4 Simulation and results

An exercise has been done to simulate RFI in RISAT-1 image.The main intent behind the exercise is to analyse the impact of RFI on high resolution image of RISAT-1 in C-band. RISAT-1 image of dumping orbit 7904, FRS-1 mode, Scene 4 acquired over Ahmedabad, Gujarat is considered for RFI simulation. Original range spectrum $H(t,f)$ of the image is shown in Figure 2. Section of original image formed is shown in Figure 3. For the purpose of RFI simulation, raw data corresponding to, ALP-SRP052920440 of ALOS

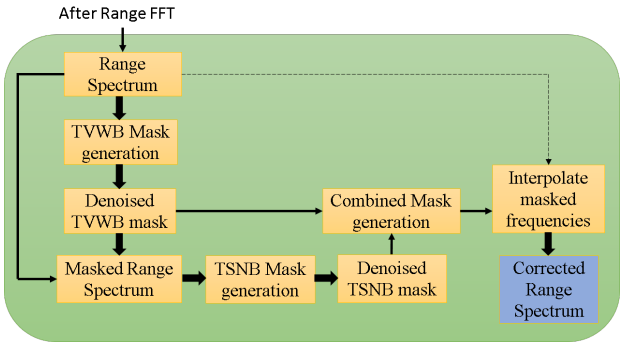

Figure 1. RFI detection and mitigation flowchart

PALSAR acquired over Nabta Playa in the south of Egypt is downloaded from the website. RFI mask extracted from ALOS data using the RFI detection algorithm is shown in Figure 4. This mask is applied on range spectrum, $H(t,f)$ of RISAT image and the masked frequencies are interpolated as discussed earlier in subsection 2.3. The new range spectrum as can be seen in Figure 5 , now consists of both TSNB and TVWB RFI. The image formed again after introducing RFI is illustrated in Figure 6. The algorithm discussed in section 4 is now applied on RFI affected range spectrum and masked range spectrum is presented in Figure 7. It can be seen from Figure 7 that majority of TVWB RFI is detected and removed from the range spectrum and only residual TSNB is left. Image formed after correcting the range spectrum is displayed in Figure 8. In order to quantitatively analyse the impact of algorithm on image quality, ten homogeneous regions of corrected image and original image are considered. Mean and standard deviation for ten regions is computed in power and scatter plot is depicted in Figure 9a and Figure 9b. Mean and SD values are downscaled by a factor of 10^{12} for display. Further, ratio of standard deviation and mean is depicted in Figure 10a. To verify that the mean value of the original image is restored after the detection and correction algorithm is implemented, mean values for the ten regions is shown in Figure 10b. SNR for these regions is tabulated in Table1.

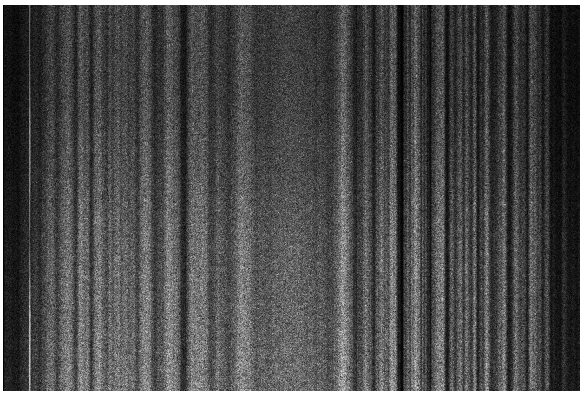

Figure 2. Range Spec. $H(t,f)$ of original image RISAT-1, dumping orbit 7904, FRS-1 mode, Scene 4

Table 1. Signal to noise ratio comparison between original and corrected images

Original Image(dB)	RFI introduced Image(dB)	Corrected Image(dB)
13.5034	-13.0274	12.5214
18.4636	-8.1867	17.3620
17.7604	-8.9399	16.6088
22.0506	-4.6282	20.9205
14.0102	-12.5877	12.9610
18.8632	-7.7974	17.7513
19.0240	-7.7052	17.8436
16.7169	-9.8822	15.6666
14.6708	-11.9616	13.5871
19.9837	-6.6695	18.8792

Figure 3. Section of original image of RISAT-1, dumping orbit 7904, FRS-1 mode, Scene 4

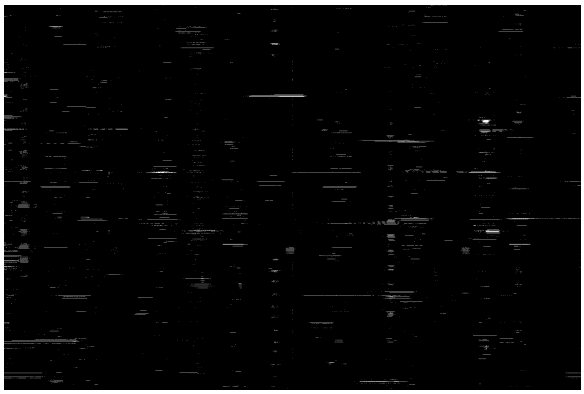

Figure 4. Generated Mask image from ALOS Image frame ALP-SRP052920440

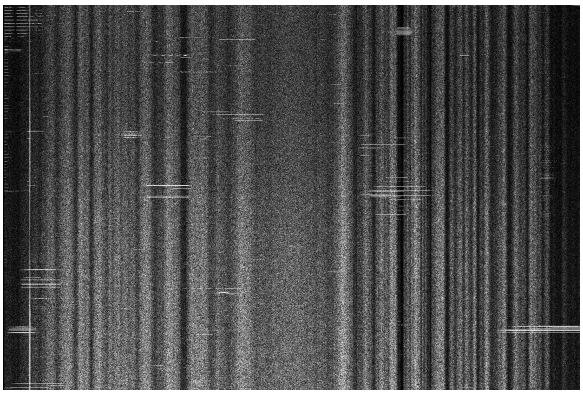

Figure 5. Range Spec. $H(t,f)$ after applying RFI mask

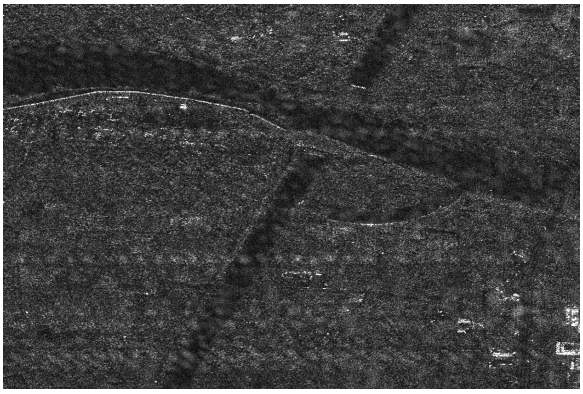

Figure 6. Section of RISAT-1 image formed after RFI insertion

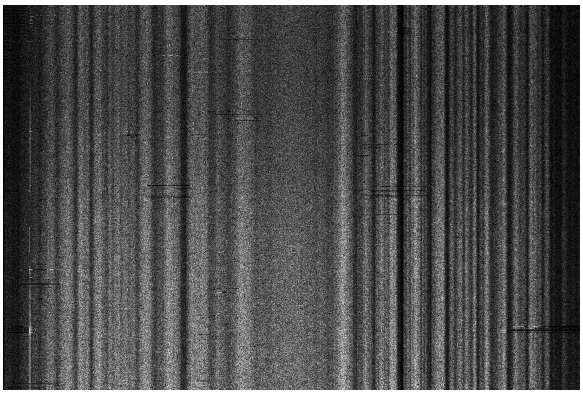

Figure 7. Range Spec. $H(t,f)$ after detecting and masking RFI

5 Conclusion

The robustness of this method comes from the fact that the detection thresholds are determined dynamically rather than assuming fixed values. Substantial improvement is observed on applying the current algorithm on simulated RFI image for RISAT-1 in Figure 6. Though the algorithm detects and removes majority of TVWB and TSNB RFI, only residual TSNB remains, same can be inferred from Figure 7. Statistical analysis of image in terms of mean and standard deviation as shown in Figure 9a, Figure 9b, Figure 10a and Figure 10b conveys that data distribution is preserved before and after RFI correction. Hence, the overall radiometric quality of image is enhanced. The same is conveyed from Table 1. It can be concluded that the algorithm provides a robust method for detecting and mitigating RFI signatures present in SAR images to a significant extent. The algorithm has been tested on few ALOS PALSAR datasets

Figure 8. Section of RISAT-1 image formed after RFI correction

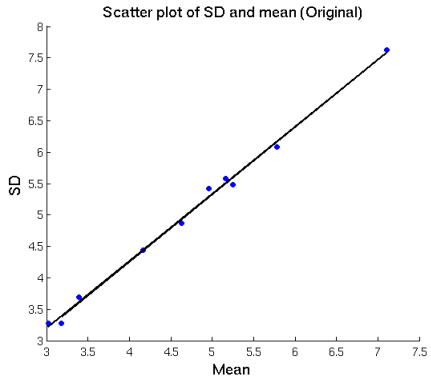

(a) Original image

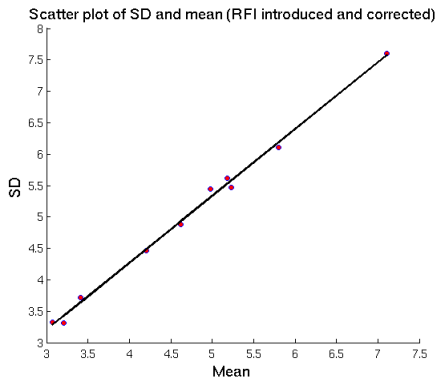

(b) Corrected image

Figure 9. SD vs mean scatter plot for original and RFI corrected image

and significant improvements have been observed. The algorithm will be useful considering the future SAR missions like NASA-ISRO joint L and S-band SAR (NISAR).

6 Acknowledgements

The authors would like to thank Alaska Satellite Facility for providing ALOS PALSAR data for this paper.

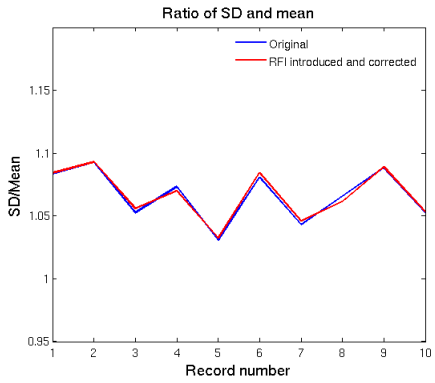

(a) SD/Mean for original and RFI corrected data

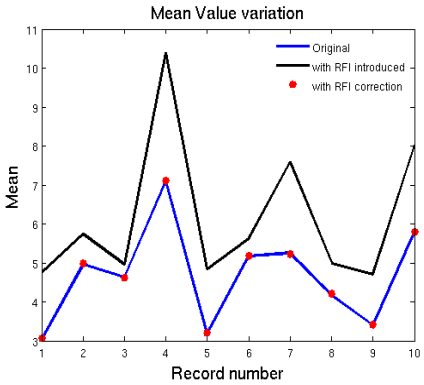

(b) Mean Values in different regions in the original image, RFI introduced and RFI corrected image

Figure 10. SD/Mean plot and mean value variation

References

[1] National Academies of Sciences, Engineering, and Medicine 2015, "A Strategy for Active Remote Sensing Amid Increased Demand for Radio Spectrum," *Washington, DC: The National Academies Press*

[2] F. J. Meyer, J. Nicoll, and A. P. Doulgeris, "Correction and Characterization of Radio Frequency Interference Signatures in L-Band Synthetic Aperture Radar Data," *IEEE Transactions on Geoscience and Remote Sensing*,Vol. 51, No. 10, October 2013.

[3] John Sacs, Hong Kong, "Robust dual scaling with Tukey's Biweight," *Applied Pshycological Measurement*,Vol. 18, No. 4, December 1994, pp. 301–309.

[4] Mendalhall W., Beaver R.J,Beaver B.M, "Introduction to probability and statistics," *Brooks/Cole cengage learning*, 14th edition, 2013, pp. 291–298.